

<https://doi.org/10.1038/s42003-025-09362-4>

Task-invariant anterior-to-posterior large-scale phase gradients of electrocorticogram oscillations during picture naming and wrist extension

Check for updates

Naoyuki Sato¹ ✉, Akihiro Shimotake^{2,3}, Mayumi Otani^{2,4}, Takayuki Kikuchi⁵, Takeharu Kunieda⁶, Ryoosuke Takahashi², Akio Ikeda⁷ & Riki Matsumoto^{2,4} ✉

Electrocorticogram (ECoG) recordings during rest have shown that theta and alpha oscillations on the cortical surface form “cortical traveling waves” across large-scale brain networks, known as phase gradients. Theoretically, these large-scale phase gradients are thought to contribute to asymmetric coupling among cortical regions. During cognitive tasks, such large-scale gradients presumably support flexible information transfer between task-related cortices; however, this has not been extensively evaluated. Here, we examined the large-scale phase gradients of ECoG theta–alpha (7 Hz) oscillations during picture naming and wrist extension tasks. Notably, large-scale anterior-posterior phase gradients that spontaneously appeared from the anterior temporal lobe (ATL) to posterior regions were only weakly dependent on task type. Nonetheless, the degree of synchronization (termed “relative phase polarity”) in task-relevant regions was significantly modulated after stimulus and movement onsets. Moreover, increased local synchronization to the traveling waves was associated with enhanced phase-dependent high-gamma activity, possibly reflecting information processing within these areas. These results suggest that task-invariant anterior-to-posterior phase gradients continuously support asymmetric coupling within a widely distributed cortical network involving the ATL and other regions and that this coupling is regulated by task-relevant regions through modulation of their local synchrony with the traveling waves.

Electrocorticography (ECoG) is a powerful technique for evaluating human cortical interactions, with high spatial and temporal resolution. Recently, ECoG studies have demonstrated that alpha and theta oscillations form “traveling waves” or “phase gradients” on cortical surfaces (gyri)^{1–6}. According to the updated version of the communication-through-coherence theory⁷, which incorporates inter-areal delays^{8,9}, phase-lagged oscillations are thought to regulate information transfer between connected regions in accordance with their conduction delay. Similarly, connectome-based neural network simulations have also predicted that theta-alpha wave propagations could contribute to asymmetric information transmission between cortices in large-scale networks based on their phase lags¹⁰. This

raises the question of whether the phase gradients in a large-scale network change during cognitive tasks according to their functional demands associated with the subprocesses in each local brain region. This remains unclear from previous evidence measured during rest^{1,2,4,5} and evidence of memory performance-dependent local direction of ECoG traveling waves, which were evaluated only in local regions (median cluster radius: 25 mm)^{3,6}. According to our connectome-based neural network simulation, the phase gradients were predicted to be organized in multiple spatial scales; global waves (> 50 mm) are associated with the coordination of empirically obtained resting-state networks (e.g., default mode network), and local radial waves (< 50 mm) are associated with coordination within these

¹Future University Hakodate, Hakodate-Shi, Hokkaido, Japan. ²Department of Neurology, Kyoto University Graduate School of Medicine, Kyoto, Japan.

³Department of Neurology, National Hospital Organization Utano National Hospital, Kyoto, Japan. ⁴Division of Neurology, Kobe University Graduate School of Medicine, Hyogo, Japan. ⁵Department of Neurosurgery, Kyoto University Graduate School of Medicine, Kyoto, Japan. ⁶Department of Neurosurgery, Ehime University Graduate School of Medicine, Ehime, Japan. ⁷Department of Epilepsy, Movement Disorders and Physiology, Kyoto University Graduate School of Medicine, Kyoto, Japan. ✉e-mail: satonao@fun.ac.jp; matsumoto@kuhp.kyoto-u.ac.jp

empirical networks¹⁰. Therefore, it would be interesting to clarify how the phase gradients in large-scale networks change during cognitive tasks.

ECoG has been a dominant tool for investigating semantic memory: general knowledge of objects, word meanings, facts, and people without connection to any particular time or space¹¹, thus semantic memory would be a good example for the evaluation of task-dependent phase gradients. Among a neural network associated with semantic memory, the anterior temporal lobe (ATL) was shown to play a dominant role in multimodal semantic integration^{12–14} and built “coherent concepts”¹⁵ in cooperation with other associated regions representing modality-specific semantic information^{16,17}. Prior ECoG studies using visual and auditory naming tasks also demonstrated that the ATL was activated several hundred milliseconds after stimulus onset, following activation in the sensory cortices¹⁸, where the semantic information was shown to be associated with both the slow potentials¹⁹ and high-gamma (70–110 Hz) activities²⁰ in the ATL. In a more recent proposal termed the “controlled semantic cognition” framework, the interaction between the semantic representation hub in the ATL and the semantic control network, including the prefrontal cortex, posterior middle temporal gyrus, and intraparietal sulcus, was proposed to be essential for the generation of context-relevant behavior²¹. Expanding on that, using an ECoG cross-spectral analysis, we demonstrated that high-gamma and slower oscillations form different networks reflecting subprocesses during picture naming, where both are associated with earlier and later processes of picture naming, respectively²². Taken together, these findings suggest that information is transferred successively from the posterior parahippocampal region, ATL, and posterior middle temporal gyrus during picture naming, providing a useful probe for how ECoG waves support in information transfer in large-scale networks.

Here, we investigated the phase gradients of theta-alpha ECoG waves on a large-scale cortical surface using data recorded during picture naming¹⁸ and evaluated the possible functional contribution of the cortical waves in the large-scale cortical network. We hypothesized that traveling waves support successive information transfer among the posterior parahippocampal region, ATL, and posterior middle temporal gyrus, consistent with the communication-through-coherence theory incorporating interareal delays^{8,9}.

Results

Relative phases during picture naming

First, we calculated the time–frequency power of the ECoG data recorded from 10 patients during picture naming, measured from 902 electrodes covering the frontal, parietal, and temporal lobes (Fig. 1a) (mean, 90 electrodes; range, 56–123 electrodes per participant) (see Supplementary Information for details of electrode locations (Supplementary Table 1) and participants (Supplementary Table 2)). There were clear peaks in the ECoG-normalized amplitude (where the 1/f background signal was removed^{13,6} only for detecting the peaks) in the theta–alpha band (7 Hz) (Fig. 1b), similar to those in previous reports^{6,23} (also see time–frequency power shown in Supplementary Fig. 1). This suggested that the theta–alpha oscillations are most likely associated with phase gradients distributed in large-scale cortical networks. Thus, in the following analyses, we focused on the phase-lag pattern of 7 Hz oscillations for all individuals, where the individual phase-lags commonly correspond to identical axonal conduction delays underlying cortical information transfer.

Topographic patterns of oscillation phases were evaluated using “relative phases”²⁴, where individual phases were compared with the average phase of all electrodes’ signals, resulting in the calculation of stable phase-lags along the time series (Fig. 1c). Figure 1d–f show an example of relative phases in a time series: 7 Hz oscillations of individual signals (Fig. 1d) were calculated using the complex Morlet wavelet, individual phases (Fig. 1e) were compared with the average phase of all signals, and the relative phases were calculated. A heat map (Fig. 1f), representing a histogram of the number of electrodes with specific relative phases at each time point, showed that the phases of many signals were synchronized with zero lag; however, the individual signals exhibited preferred relative phases (Fig. 1g).

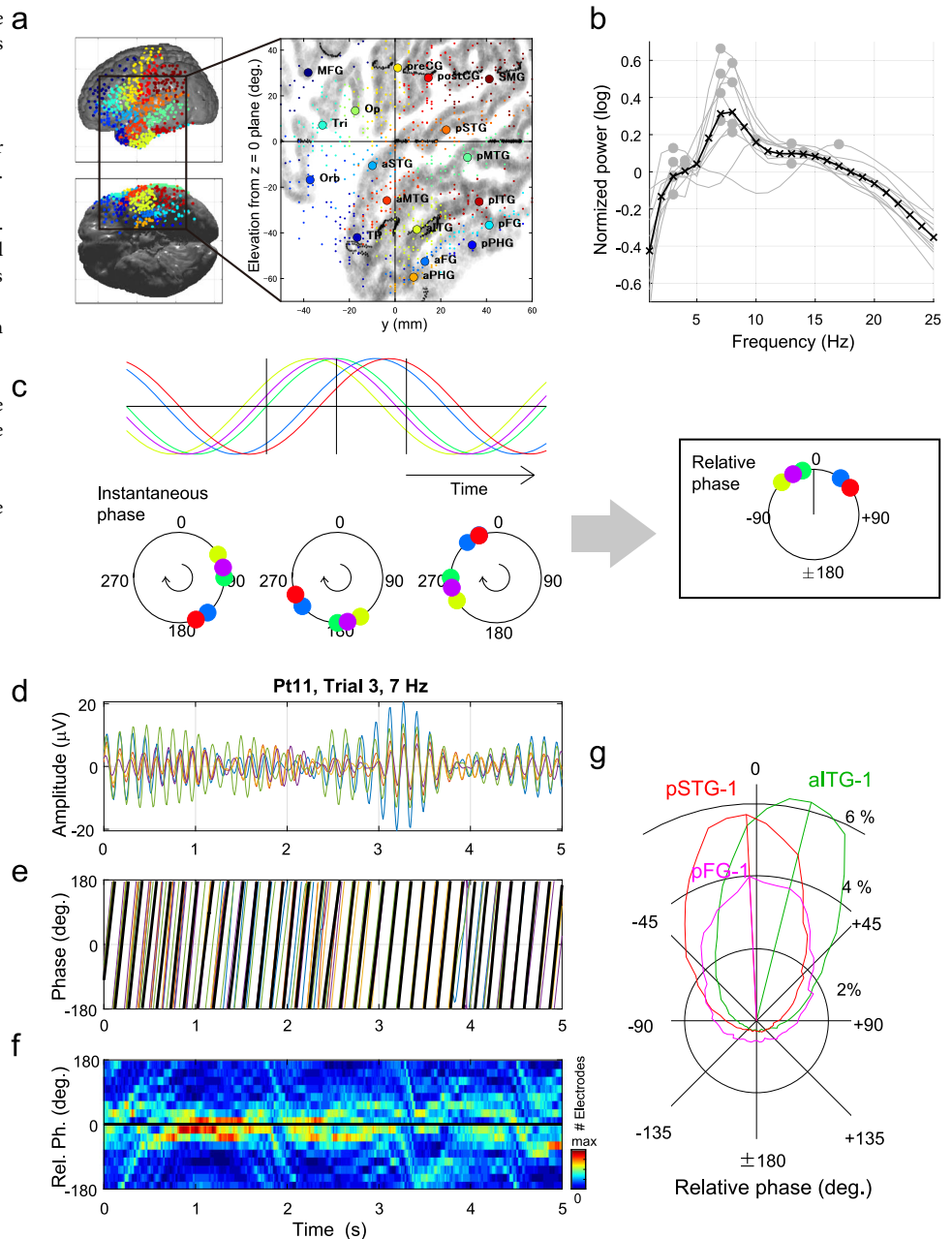
Figure 2a shows the spatial distribution of relative phases of all individual electrodes, revealing an anterior-to-posterior large-scale phase gradient, where the ventral ATL exhibited advanced phases, whereas delayed phases were observed in the posterior temporal region (see Supplementary Fig. 2 for individual spatial distributions of relative phases). At the same time, local phase gradients in the superior and ventral parts of the temporal lobe were also observed along the dorsal–ventral axis. Figure 2b demonstrates the orientation of these phase gradients for each participant, showing that the anterior-to-posterior phase gradients were common across all participants (Rayleigh’s test for circular uniformity: Rayleigh’s $z = 4.22$, $p = 0.01$) (see Supplementary Fig. 2 for individual angular distributions of phase gradient orientation). The average phase propagation speed was 3.5 m/s (Fig. 2c), aligning with a previous report (2–5 m/s) and slightly exceeding other reports (< 1 m/s)^{2,3,6}; both are considered within the range of axonal conduction delays²⁵. The wavelength was 24.5 cm, indicating that detailed anatomical structures, such as gyri and sulci, likely have minimal impact on the calculation of the phase gradient.

To perform across-participant analyses, we defined 18 region of interests (ROIs) covering the frontal, parietal, and temporal lobes (Fig. 1a) and calculated the temporal evolution of relative phases during picture naming in each ROI. Relative phases in each ROI and time point were statistically evaluated using a combination of sign tests for “polarity (in-phase or out-phase)” and “sign (advanced or delayed phases)” of the relative phases; these statistical values were then averaged in the group analysis (Fig. 3a, b) (see Supplementary Fig. 3 for individual relative phases). Notably, the phase pattern across the ROIs appeared roughly constant over time, suggesting similar phase gradients at every time point (including the pre-stimulus period) (for polarity: maximum value of $Z = 27.6$, $p < 10^{-6}$, at 1.2 s, at the temporal pole (TP); for sign: maximum value of $Z = 9.20$, $p < 10^{-6}$, at 1.5 s, at TP), which is known to be associated with semantic information processing in the ATL^{18–20} clearly demonstrates the phase gradients, with advanced phases in the ATL and delayed phases in other posterior regions.

Subsequently, event-related changes in the relative phases from baseline (–0.2–0 s before picture onset) were evaluated. During 0.5–1 s after stimulus onset, the in-phase polarities of the relative phases were significantly increased in the ventral temporal regions, including the anterior and posterior fusiform gyri (aFG and pFG), posterior inferior temporal gyrus (pITG), and posterior parahippocampal gyrus (pPHG) (maximum value of $Z = 4.73$, $p = 0.003$, at 0.7 s, at pFG), while the out-phase polarities of the relative phases were significantly increased in the anterior and posterior middle temporal gyrus (aMTG and pMTG) (maximum value of $Z = 3.87$, $p = 0.0001$, at 0.6 s, at pMTG) (Fig. 3e, f). However, notably, the signs of the relative phases in each ROI did not change significantly from the baseline after picture onset. The influence of the selection of the peak frequency (7 Hz) was additionally tested but was found to be minimal (see Supplementary Fig. 4). These results do not directly support our initial hypothesis that the traveling wave supports successive information transfer among the posterior parahippocampal region, the ATL, and the posterior middle temporal gyrus during semantic processing. Instead, the results suggest that the modulation of local synchrony to the traveling waves in these regions (including pPHG, aFG, and pMTG) is associated with semantic processing.

The articulation-related changes of the relative phases were also elevated, with onset times defined on a trial-by-trial basis (average participant response time was 1.75 s; see Supplementary Table 2 for details). After articulation, the in-phase polarities of the relative phases were significantly increased in the postcentral gyrus (postCG), aMTG, pMTG, and the anterior and posterior superior temporal gyri (aSTG and pSTG) (maximum value of $Z = 3.58$, $p = 0.0003$, at 1.5 s, at aSTG), while the out-phase polarities were significantly increased in the pFG and pPHG (maximum value of $Z = 4.52$, $p < 10^{-5}$, at 0.7 s, at pFG) (Fig. 3g, h). The signs of the relative phases in each ROI remained largely unchanged, suggesting that while polarities were modulated by subprocesses of picture naming, their overall direction did not change.

Fig. 1 | Relative phase analysis. **a** Specific electrode locations within 18 ROIs. A topographical map was calculated using a cylindrical projection with anterior-posterior axis (y-axis in MNI coordinate) to show electrode locations covering the lateral to ventral part of the cortex. **b** Averaged spectral power (normalized) of ECoG signals from 10 participants. Filled circles denote peaks in individual plots. The black line denotes the average of all individual plots. **c** Calculation of relative phases. Phases of each signal advance as time goes on, while their relative phases are more stable in time. **d, e, f** Example of the calculation of relative phases. Signals were filtered with a center frequency of 7 Hz (**d**), and instantaneous relative phases of signals from all electrodes were calculated, where bold black lines show their average phases (**e**). A heat map (**f**) shows the histogram of the instantaneous relative phases of all electrodes. **g** Angular distribution of instantaneous relative phases of three electrodes. The radius represents the frequency of the appearance of relative phases at each angle.



To confirm the weak modulation of the relative phases by task events, we further tested the difference in relative phases after stimulus onset between faster and slower responding trials (no baseline correction). We found no significant differences in either the signs or polarities of the relative phases, suggesting that relative phases are not strongly modified by cognitive load during picture naming.

Relative phases during wrist extension

To test whether the phase gradients were comparably stable during other tasks besides picture naming, we examined data from a voluntary wrist extension task, in which participants were asked to make self-paced movements of the right wrist (median movement interval: 13.4 s). Wrist extension was chosen because it requires cognitive demands sufficiently different from those of picture naming. We additionally analyzed ECoG data during voluntary wrist extension in 6 of the 10 participants included in the picture-naming analysis. Figure 4a and b show the results of the relative phases in each ROI and the time after initiation of wrist movement.

Similarly, the topographical map of the relative phases revealed a gradient advancing from the ATL to posterior regions (Fig. 4c, d) (maximum value of $Z = 10.67, p < 10^{-6}$, at 2.3 s, at TP). Event-related changes of relative phases from baseline (-0.2–0 s before movement onset) showed significantly increased in-phase polarities of the relative phases in the postCG 0.4–0.7 s after wrist movement (maximum value of $Z = 4.66, p < 10^{-5}$, at time of 0.7 s, at postCG) with no changes in the signs of the relative phases from baseline (Fig. 4e, f).

The differences in relative phases between the two tasks appeared minimal, raising the question of whether these differences are truly task-related. To compare phase gradients between the two tasks, the differences in relative phases were first calculated individually, and then integrated for group analysis. Figure 5a shows the difference in relative phase polarities after picture onset and wrist movement onset (maximum value of Z for picture onset = 8.20, $p < 10^{-6}$, at 0.6 s, at pFG; maximum value of Z for movement onset = -3.71, $p < 0.0005$, at 0.7 s, at postCG). This result likely reflects as a combination of event-related changes after picture onset

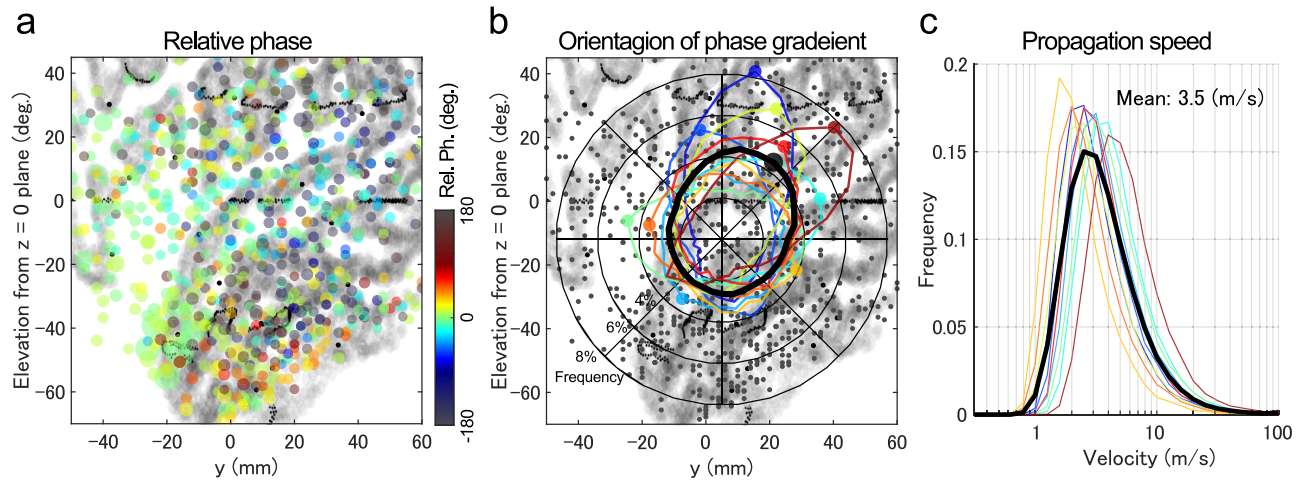


Fig. 2 | Spatial distribution of relative phases. **a** Overall distribution of relative phases of all electrodes, where the relative phase was given by the mode value in the angular histogram with a bin of 22.5 degrees during all task periods. Location of each circle indicates electrode location, and its color denotes the value of the relative phase, where red and blue indicate advanced and delayed phases. **b** Individual angular distribution of phase gradient orientation with a bin of 22.5 degrees. Colors

represent individuals, where lines represent the frequency of phase gradient orientation, and dots represent mode values in the angular distribution. A bold black plot shows the average result. Black dots on the map denote electrode locations. **c** Individual distribution of propagation speed. Colored lines show individual results, and a bold black line shows the average result.

(Fig. 3e) and wrist movement onset (Fig. 4e). The pre-stimulus phase polarity difference in pFG may reflect differences in preparatory activity, likely owing to the fixed 5-s interval of picture presentations versus the self-paced wrist extensions. Figure 5b demonstrates the difference in relative phase polarities after articulation onset and wrist movement onset (maximum value of Z for articulation onset = 5.28, $p < 10^{-6}$, at 0.2 s, at pFG; minimum value of Z for movement onset = -3.97, $p < 0.0001$, at 0.9 s, at SMG). Additionally, we evaluated differences in phase polarities after picture and articulation onsets during the picture-naming task (Fig. 5c), where multiple ROIs, including pFG and aMTG, showed significant changes before the event onsets (maximum value of Z = 6.29, $p < 10^{-6}$, at 0.7 s, at pFG; maximum value of Z = -4.52, $p < 10^{-5}$, at -0.3 s, at pFG). In all three comparisons, the signs of the relative phases were not significantly different between the two tasks. These results again suggest that phase polarities are modulated by task events (including semantic processing, articulation, and self-paced movement) but not phase signs.

Relationship between relative phases and theta-alpha and high-gamma amplitudes

According to the communication-through-coherence theory with interareal delays^{8,9}, the lagged, slow oscillations between connected regions are expected to contribute to the asymmetric transfer of information via neural firing across these regions. Previous ECoG reports have demonstrated high-gamma amplitude modulation by slow oscillation phases^{23,26}. Thus, it is of interest to determine whether high-gamma amplitudes are correlated with theta-alpha phases during picture naming. We evaluated this using a phase-amplitude coupling (PAC) analysis. The results (Fig. 6a) showed that high-gamma amplitudes in each ROI over the entire period were significantly correlated with theta-alpha phases, peaking at the out-phase of the theta-alpha phase (-171.2° on average). In the event-related analysis, PAC (Fig. 6b) was significantly increased in the aFG, pITG, pFG, and pPHG at around 0.5 s and in the preCG and postCG at 0.5–2.2 s. In summary, these findings show that theta-alpha phases spontaneously couple with high-gamma amplitudes; however, task-dependent increases in these couplings were significantly correlated with increases in in-phase polarity after stimulus presentation onset (Fig. 3e) (correlation coefficient: 0.35, $p < 0.01$).

Discussions

We demonstrated the novel phenomena of task-invariant ECoG anterior-to-posterior large-scale phase gradients during picture naming and wrist

extension tasks. Our findings did not completely validate our initial hypothesis that phase gradients support the successive information transfer among the posterior parahippocampal region, ATL, and posterior middle temporal gyrus. The spatial direction of the observed phase gradients appeared consistent with the prior ECoG evidence during rest² and sleep⁵ and with computer simulations using connectome-based neural networks^{10,27}. Thus, this pattern was likely a type of spontaneous structure originally derived from the cortical network structure, as also supported by the significant correlation between cortical laminar structures and the theta-band frequency gradients from the anterior-to-posterior regions²⁸. According to the communication-through-coherence theory with interareal delays^{8,9}, information transfer from the aFG to the pMTG (approximate distance of 5.4 cm) with a 15.3 ms delay would be facilitated by propagation waves travelling at 3.5 m/s, provided that both activities are synchronized in-phase with the propagation waves. The current result demonstrates that this type of information transfer from ATL to other regions can be supported by the task-invariant anterior-to-posterior phase gradients.

The polarities of the relative phases (i.e., in-phase and out-phase) were modified in response to the stimulus and movement onsets from baseline, which can be thought to regulate the information transfer supported by the propagation waves. When the local activity in a region is in-phase (or out-phase), that region will be included (or excluded) in the anterior-to-posterior unidirectional couplings with other regions. Accordingly, in picture naming (Fig. 3d), the anterior-to-posterior information transfer during 0.4–1.1 s after stimulus onset was facilitated in the ventral region of the temporal lobe (pPHG, aFG, pFG, and pITG), which had increased in-phase activities, but not in the regions in the middle temporal gyrus (the pMTG and aMTG) having the increased out-phase activities. Per our initial hypothesis, the former is thought to reflect the feedback signal from the ATL semantic hub to regions maintaining modality-specific information^{14,16}, and the latter is thought to be an independent process associated with the semantic control network producing a correct response²¹. Note that these locations and periods are consistent with prior ECoG evidence during picture naming where semantic information was represented by slow¹⁹ and high-gamma activities in the ATL²⁰ within a period of several hundred milliseconds after stimulus onset.

In agreement with a previous report²³, the high-gamma amplitudes in our study were strongly coupled with theta-alpha phases in every ROI during picture naming (Fig. 6a). Thus, information transfer of high-gamma

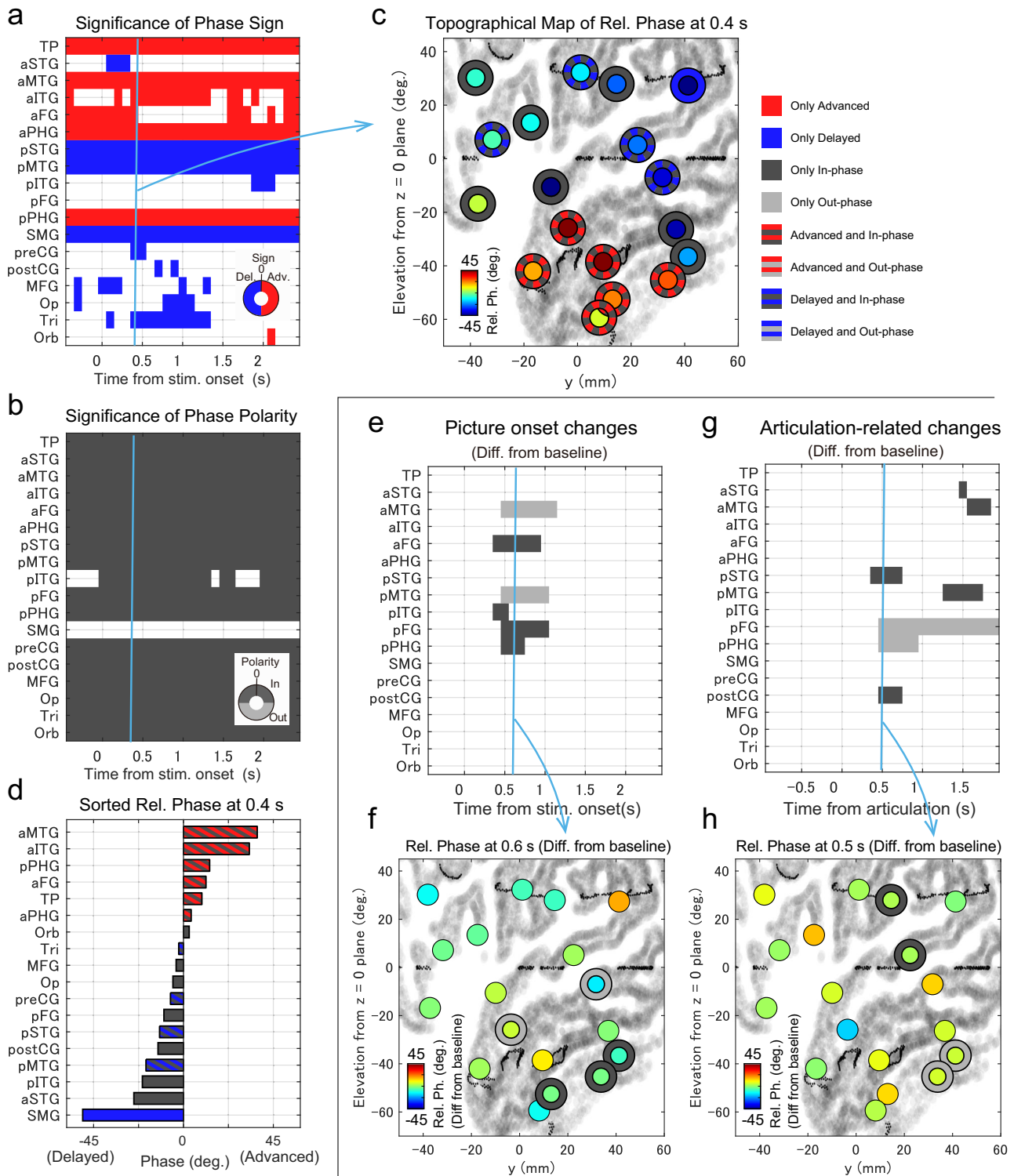


Fig. 3 | Relative phases during picture naming task. **a, b** Significant appearance of relative phase sign (advance (red) or delay (blue)) (**a**) and relative phase polarity (in-phase (dark gray) or out-phase (light gray)) (**b**) for each ROI and time ($p < 0.05$). The colored circle in the bottom right of the figures summarizes these color indices. “Adv.” and “Del.” denote “Advance” and “Delay”, respectively. The white area denotes no significance. **c** Topographical map of the relative phases at 0.4 s after picture presentation onset. Circles indicate the locations of each ROI, where the fill color indicates the relative phases at each ROI. Bold edges represent the significant appearance of the positive and negative signs (advance (red) or delay (blue)) and/or polarities of the relative phases (in-phase (dark gray) or out-phase (light gray)), using the identical color indices in (**a**) and (**b**). Colored border pattern denotes their

combination (advance and in-phase (red and dark gray), delay and in-phase (blue and dark gray), advance and out-phase (red and light gray), and delay and out-phase (blue and light gray)). **d** Sorted relative phases at 0.4 s after picture onset presentation. The filled colors of the bars indicate the significant appearance of signs and/or polarities of relative phases, with identical color indices in (**c**). **e, f** Picture onset-related changes of the relative phases from a baseline (-0.2–0 s of picture onset). Significant changes of the relative phases from the baseline are shown in a spatiotemporal map (**e**) and a topographical map (**f**) at 0.6 s after stimulus onset. **g, h** Articulation-related changes of the relative phases from a baseline (-0.2–0 s of articulation) are shown in a spatiotemporal map (**g**) and a topographical map (**h**).

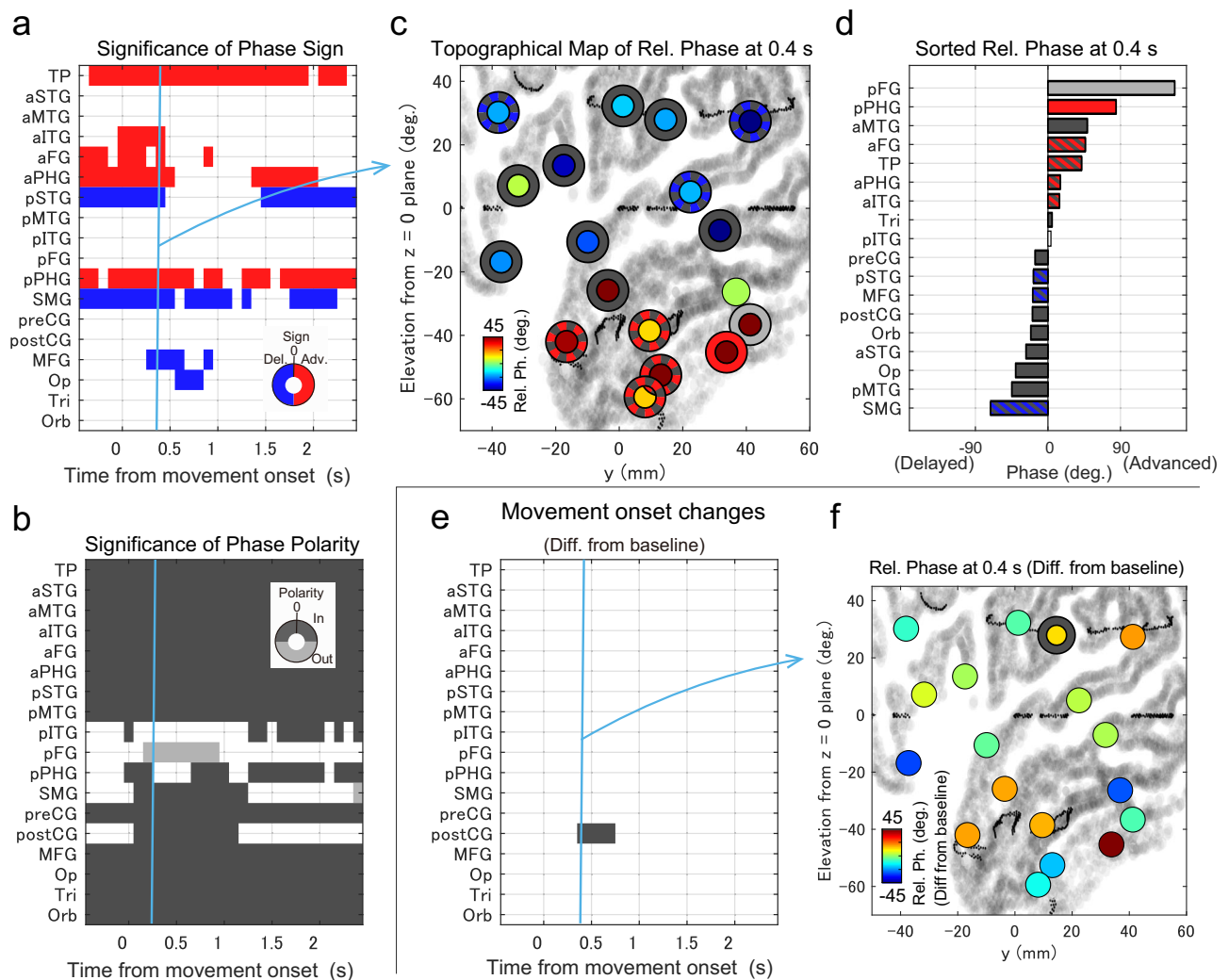


Fig. 4 | Relative phases during wrist extension task. a–d The significant appearance of positive and negative signs (a) and polarities (b) of relative phases in time series, a topographical map (c) and a plot of sorted relative phases (d) at 0.4 s after wrist movement, shown with the same format of Fig. 3. **e, f** Movement onset-related changes of the relative phases from a baseline (-0.2–0 s of movement onset) are shown in a spatiotemporal map (e) and a topographical map (f) at 0.4 s after the movement.

activities is thought to be constantly supported by theta-alpha propagation waves in the anterior-to-posterior direction. Moreover, task-dependent changes in the couplings of theta-alpha phases and high-gamma amplitudes were found in the ventral regions of the temporal lobe (aFG, pITG, pFG, and pPHG; Fig. 6b). Interestingly, these were significantly correlated with increased in-phase activities (Fig. 3e). These findings suggest that regulation of the anterior-to-posterior information transfer in a region is linked with information processing implemented by the high-gamma activity in that region.

This study had several limitations. First, the electrodes did not cover the entire cortical region; thus, the interactions between the current theta-alpha traveling waves and possible waves in other regions, such as in the contralateral temporal regions, remain to be investigated. Such information would help assess the functional roles of the traveling waves in large-scale brain networks. Second, hierarchical interactions between global (> 50 mm) and local (< 50 mm) waves, which were predicted by our computer simulation¹⁰, were not evaluated in the current analysis. In contrast to the task-invariant global waves found in the current study, local waves were reported to be modified by cognitive tasks^{3,6}. Third, the current analysis did not reject possible contamination of volume conducted signals; the ECoG signals themselves were thought to be local signals within 3 mm²⁹ or 20 mm³⁰ and the inter-ROI distance in the current study was within this

range (mean and standard deviation of the nearest neighboring ROI distance: 17.9 and 3.7 mm, respectively), while the summed activity over an extended cortical area in each ROI (mean number of electrodes/ROI/participant) could enhance possible volume conducted local signals³¹. Fourth, we focused on the group analysis of the phase gradients in the current study, while individual differences of the phase gradients were found to be large (Supplementary Figs. 2 and 3), in agreement with a previous report¹. Such variation might be important for understanding individual cognition; however, this was beyond the aim of the current study.

In conclusion, anterior-to-posterior large-scale traveling waves in the theta-alpha band were found to be task-invariant during picture naming and wrist extension. These traveling waves were suggested to support the asymmetric couplings in the widely distributed cortical network from the ATL and other regions, where these couplings are regulated by the task-relevant regions modulating their local synchrony to the traveling waves. This would generalize the communication-through-coherence theory with inter-areal delays^{8,9}, in terms of the information transfer among the continuously distributed cortical regions in the size of cortical lobes. Future investigations on the relationship between individual connectomes and their cognition dependence of traveling waves are required to uncover the traveling wave-based information integration in the large-scale cortical networks.

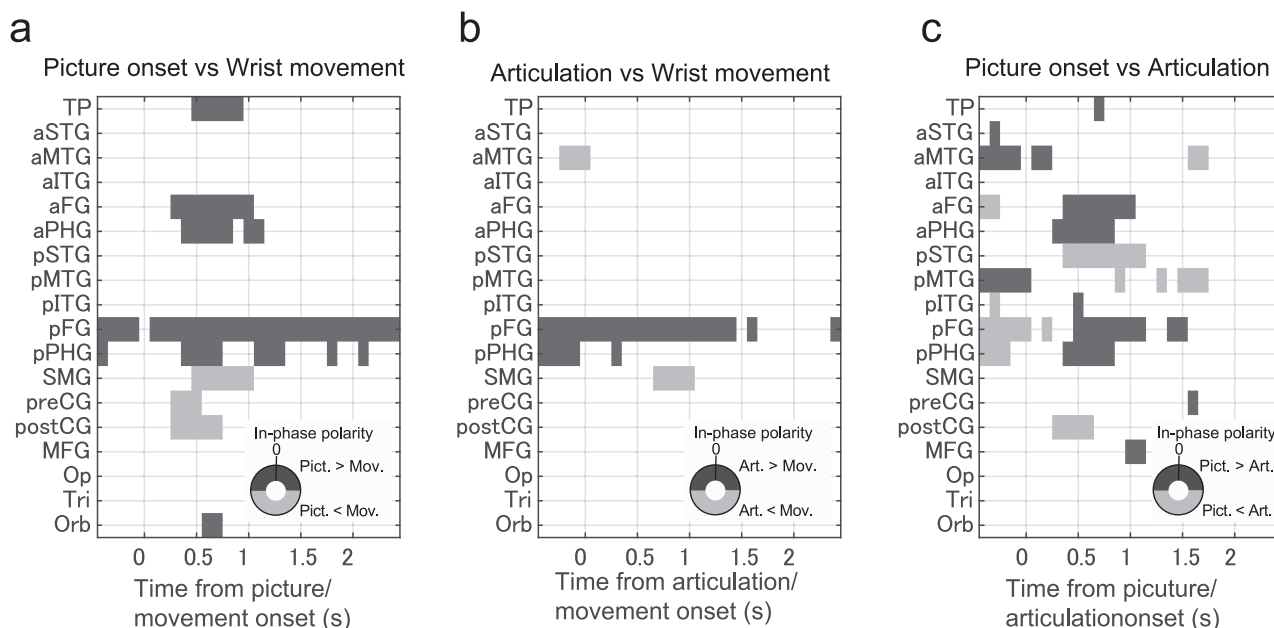
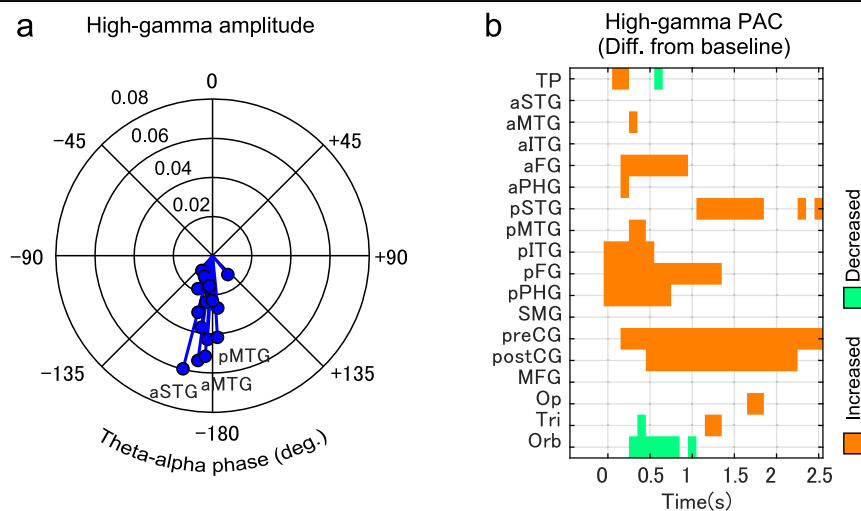


Fig. 5 | Significant differences in the relative phase polarity between different conditions (no baseline correction). **a** Differences in the phase polarity after picture onset and those after wrist movement onset. Dark gray indicates that phase polarity after picture onset was significantly tended to be in-phase in comparison to those after wrist movement. Light gray indicates that phase polarity after wrist movement

was significantly tended to be in-phase in comparison to those after picture onset. **b** Differences in the phase polarity after articulation onset and those after wrist movement onset. **c** Differences in the phase polarity after picture onset and those after articulation onset.

Fig. 6 | Coupling of theta-alpha phase and high-gamma amplitude. **a** Weighed sum of high-gamma power by theta-alpha phases in each ROI. The length represents the synchronization index of the phase-amplitude coupling (PAC). **b** Event-related PAC changes. Orange and green denote significant increases and decreases in the coupling, respectively ($p < 0.05$).



Methods

Participants and tasks

We evaluated the ECoG data used in previous studies^{18,19,22} and included 10 patients from these studies (five females, aged 17–55 years, patient IDs: Pt1–5, 7, and 9–12; patients in whom electrodes were implanted in the language-nondominant hemisphere (Pt6 and Pt8) were excluded) with intractable partial epilepsy or brain tumors. Subdural electrode implantation was performed in the language-dominant hemisphere for presurgical evaluation. The age at seizure onset was >6 years for all the participants (see Supplementary Tables 1 and 2 and the original papers^{18,22} for detailed information). All participants provided informed consent according to the protocol approved by the Ethics Committee of the Kyoto University Graduate School of Medicine (approval no. C533). All ethical regulations relevant to human research participants were followed.

Participants underwent 400 picture naming trials using 100 samples of line drawings (50 living and 50 non-living objects), where they were presented with the stimuli for 5 s (average participant response time: 1.75 s) and asked to name each item as quickly and accurately as possible. The mean number of trials analyzed was 315 per participant (range, 189–385). Further details regarding this task can be found in a previous report¹⁹. Six of the ten participants also performed a wrist extension task, where they were asked to make self-paced movement of the right wrist (or the left wrist for a patient with left-hemispheric language dominance) at a rate of approximately one movement every several seconds (mean, 116 trials; range, 96–132 trials). Details of this task were described in our previous report³².

Data acquisition

Subdural electrodes were consistently placed on the left (or right, in Patient Pt12) hemisphere, covering the frontal, parietal, and temporal lobes of each

patient (mean, 90 electrodes; range, 56–123 electrodes/patient). The electrodes were made of platinum and had an inter-electrode distance of 1 cm and a recording diameter of 2.3 mm (ADTECH, WI, USA). Electrode placement is illustrated in Fig. 1a.

ECoG signals were recorded at a sampling rate of 1000 and 2000 Hz for seven and three patients (Pt01, Pt03, and Pt05) participants, respectively. Raw data were measured with reference to the electrode beneath the galea aponeurotica in seven patients and to the scalp electrode on the mastoid process contralateral to the side of electrode implantation in three patients (patient IDs: Pt01, Pt02, and Pt03). Signals from the electrodes in the seizure onset zone were identified by a board-certified encephalographer and epileptologist (R.M. and A.S.).

Signal processing

ECoG data from the electrodes that included more than four bad trials (1% of all trials) with sharp waves (defined by >100 μV in amplitude and >75 ms in duration) were discarded, and the remaining data were reformatted into a common average reference.

The time-frequency spectrum of the ECoG time series data of the *j*-th electrode, $e_j(t)$, at time *t* with center frequency f_0 , $s_j(t, f_0)$, was calculated using the complex Morlet wavelet transformation³³, as follows:

$$s_j(t, f_0) = e_j(t) * h(t, f_0) \text{ with } h(t, f_0) = A \exp(-t^2 / (2\sigma_t^2)) \exp(2\pi i f_0 t)$$

where * denotes an operator of the convolution, $h(t, f_0)$ is a complex Morlet wavelet, σ_t is the length in the time domain (“width” was defined by $2\pi f_0 \sigma_t = 10^{34}$), *A* is constant for normalization ($= (\sigma_t \sqrt{\pi})^{-1/2}$), and *i* is the imaginary unit. Instantaneous phase of the *j*-th electrode at time *t* with center frequency f_0 , $\theta_j(t, f_0)$ was given by:

$$\theta_j(t, f_0) = \arg(s_j(t, f_0)); (-\pi, \pi]$$

where $\arg(z)$ denotes the argument of a complex number *z*, the instantaneous amplitude was given by $|s_j(t, f_0)|$. Twenty-five center frequencies were considered on a linear scale (1, 2, ..., 25 Hz).

The relative phase of the *j*-th electrode in the set of electrodes, *E*, $\Delta\theta_j(t, f_0)$ was defined by:

$$\Delta\theta_j(t, f_0) = \arg(e^{i(\theta_j(t, f_0) - \bar{\theta}(t, f_0))}) \text{ with } \bar{\theta}(t, f_0) = \arg\left(\sum_{j \in E} e^{i\theta_j(t, f_0)}\right)$$

Note that the relative phase is undefined for Rayleigh’s *R* ($R = |\sum_{j \in E} e^{i\theta_j(t, f_0)}|$) = 0 indicating that the distribution of phases is perfectly uniform. In the current analysis, the data from all time points during the tasks were analyzed, where the means of individual *R*s at 7 Hz were significantly larger than 0 in a group analysis (mean and standard deviation: 0.14 and 0.06, respectively; $t(9) = 7.2, p < 10^{-4}$).

The cross-participant analysis was performed based on 18 ROIs, as shown in Fig. 1a (see Supplementary Table 1 for detailed information). These ROIs were identical to those used in our previous report²². Data for each ROI was drawn from ≥ 6 participants (mean number of participants/ROI = 8.8, mean number of electrodes/ROI = 45.0). The relative phase for the *k*-th ROI constituting the set of electrodes *E'* is defined by $\Delta\varphi_k = \arg(\sum_{j \in E'} e^{i\Delta\theta_j})$.

Velocity of the propagation waves was calculated by the linear regression of the relative phases in a topographical plane, which was given by a cylindrical projection with anterior-posterior axis (y-axis in MNI coordinate) covering ROI locations continuously in the lateral to ventral part of the cortex. A 10 degree in the y-axis corresponded to 10.3 mm, where the radius of the cylinder was given by the mean radius of the ROI locations (59.2 mm).

The instantaneous high-gamma band amplitude was calculated using the Hilbert transform of the band-passed signal using the 4th-order Butterworth filter with a cutoff frequency of 80–120 Hz. The coupling between slow oscillation phases and high-gamma amplitude at the *k*-th ROI was evaluated using the synchronization index, given by:

$$c_k = \frac{1}{|T|} \left| \sum_{t \in T} A_k^y e^{i\varphi_k(t)} \right|$$

where *T* denotes the set of time points, A_k^y denotes the high-gamma amplitude and φ_k denotes the phase of the slow oscillations. c_k is large for a significant in-phase (or out-phase) coupling between the slow wave and high-gamma amplitude, and $c_k = 0$ for random coupling between them.

Statistics and reproducibility

Data from all-time points were analyzed to evaluate the steady properties of the relative phases regardless of their synchronies to the global waves, where the nonparametric test based on binomial distribution was used to have stable statistical value also in the case of low-synchrony data, including outliers of out-phases. The distribution of the relative phases for each ROI and time was statistically evaluated by a combination of two independent two-tailed binomial tests using Z-values³⁵ on relative phase polarity (in-phase [$|\Delta\varphi| < 0.5\pi$] or out-phase [otherwise]) and relative phase sign (advanced [$\Delta\varphi > 0$] or delayed [otherwise]). The Z-values of the *k*-th ROI and time *t* in the data of *N* trials, including N_k^A of advanced (or positive) phase trials and N_k^I of in-phase trials, are given by:

$$Z_k^A = \frac{N_k^A - 0.5N}{0.5\sqrt{N}} \text{ and } Z_k^I = \frac{N_k^I - 0.5N}{0.5\sqrt{N}}$$

where Z_k^A and Z_k^I denote the Z-values of the sign and polarity of the relative phases, respectively. These values were individually calculated and integrated into a Z-value of *M* participants’ Z-values (using the inverse normal method). Multiple comparisons (18 ROIs × 26 time points [sampled with a 0.1-s interval]) were corrected using false discovery rate (FDR) control ($q = 0.05$).

In event-related analysis, the changes in relative phases from a baseline (from -0.2 s to 0 s of the event onset) were calculated as $\Delta\varphi_k(t) = \arg(e^{i(\Delta\varphi_k(t) - \Delta\bar{\varphi}_k)})$ with $\Delta\bar{\varphi}_k = \arg(\sum_{-0.2 \leq t < 0} e^{i\Delta\varphi_k(t)})$. The distributions of the baseline-corrected relative phases were then statistically evaluated in the same fashion as the above methods.

Additionally, the group-level statistical values of the relative phase polarities in a time series were compared with the PAC synchronization indices using the permutation test of Pearson’s correlation coefficient with 2000 permutations.

Reporting summary

Further information on research design is available in the Nature Portfolio Reporting Summary linked to this article.

Data availability

All source data underlying the graphs and charts presented in the main and Supplementary Figs. are provided in Supplementary Data. The datasets that support the findings of this study are available from the corresponding author upon reasonable request.

Code availability

For data analyses standard MATLAB subroutines (wavelet analysis, signal filtering, statistical values) are used in a particular order as explained in the Methods section of the paper.

Received: 8 September 2025; Accepted: 2 December 2025;

Published online: 20 December 2025

References

- Bahramisharif, A. et al. Propagating neocortical gamma bursts are coordinated by traveling alpha waves. *J. Neurosci. : Off. J. Soc. Neurosci.* **33**, 18849–18854 (2013).
- Halgren, M. et al. The generation and propagation of the human alpha rhythm. *Proc. Natl. Acad. Sci. USA* **116**, 23772–23782 (2019).
- Mohan, U. R., Zhang, H., Jacobs, J.: The direction and timing of theta and alpha traveling waves modulate human memory processing. (2022)
- Muller, L., Chavane, F., Reynolds, J. & Sejnowski, T. J. Cortical travelling waves: mechanisms and computational principles. *Nat. Rev. Neurosci.* **19**, 255–268 (2018).
- Muller, L. et al. Rotating waves during human sleep spindles organize global patterns of activity that repeat precisely through the night. *Elife* **5**, (2016)
- Zhang, H., Watrous, A. J., Patel, A. & Jacobs, J. Theta and Alpha Oscillations Are Traveling Waves in the Human Neocortex. *Neuron*. **98**, 1269–1281.e1264 (2018).
- Fries, P. A mechanism for cognitive dynamics: neuronal communication through neuronal coherence. *Trends Cogn. Sci.* **9**, 474–480 (2005).
- Bastos, A. M., Vezoli, J. & Fries, P. Communication through coherence with inter-areal delays. *Curr. Opin. Neurobiol.* **31**, 173–180 (2015).
- Fries, P. Rhythms for Cognition: Communication through Coherence. *Neuron*. **88**, 220–235 (2015).
- Sato, N.: Cortical traveling waves reflect state-dependent hierarchical sequencing of local regions in the human connectome network. *Scientific reports* **12**, (2022)
- Tulving, E.: Episodic and semantic memory. In: Tulving, E., Donaldson, W. (eds.) *Organization of Memory*. Academic Press (1972)
- Binney, R. J., Embleton, K. V., Jefferies, E., Parker, G. J. & Lambon Ralph, M. A. The ventral and inferolateral aspects of the anterior temporal lobe are crucial in semantic memory: evidence from a novel direct comparison of distortion-corrected fMRI, rTMS, and semantic dementia. *Cereb. cortex* **20**, 2728–2738 (2010).
- Lambon Ralph, M. A., Sage, K., Jones, R. W. & Mayberry, E. J. Coherent concepts are computed in the anterior temporal lobes. *Proc. Natl. Acad. Sci. USA* **107**, 2717–2722 (2010).
- Patterson, K., Nestor, P. J. & Rogers, T. T. Where do you know what you know? The representation of semantic knowledge in the human brain. *Nat. Rev. Neurosci.* **8**, 976–987 (2007).
- Lambon Ralph, M. A. Neurocognitive insights on conceptual knowledge and its breakdown. *Philos. Trans. R. Soc. Lond. Ser. B, Biol. Sci.* **369**, 20120392 (2014).
- Rogers, T. T. et al. Structure and deterioration of semantic memory: a neuropsychological and computational investigation. *Psychological Rev.* **111**, 205–235 (2004).
- Lambon Ralph, M. A., Lowe, C. & Rogers, T. T. Neural basis of category-specific semantic deficits for living things: evidence from semantic dementia, HSVE and a neural network model. *Brain : a J. Neurol.* **130**, 1127–1137 (2007).
- Shimotake, A. et al. Direct exploration of the role of the ventral anterior temporal lobe in semantic memory: Cortical stimulation and local field potential evidence from subdural grid electrodes. *Cereb. cortex* **25**, 3802–3817 (2015).
- Chen, Y. et al. The ‘when’ and ‘where’ of semantic coding in the anterior temporal lobe: Temporal representational similarity analysis of electrocorticogram data. *Cortex; a J. devoted study Nerv. Syst. Behav.* **79**, 1–13 (2016).
- Rupp, K. et al. Semantic attributes are encoded in human electrocorticographic signals during visual object recognition. *Neuroimage* **148**, 318–329 (2017).
- Lambon Ralph, M. A., Jefferies, E., Patterson, K. & Rogers, T. T. The neural and computational bases of semantic cognition. *Nat. Rev. Neurosci.* **18**, 42–55 (2017).
- Sato, N. et al. Frequency-Dependent Cortical Interactions during Semantic Processing: An Electrocorticogram Cross-spectrum Analysis Using a Semantic Space Model. *Cereb. cortex* **31**, 4329–4339 (2021).
- Canolty, R. T. et al. High gamma power is phase-locked to theta oscillations in human neocortex. *Science* **313**, 1626–1628 (2006).
- Alexander, D. M., Trengove, C., Wright, J. J., Boord, P. R. & Gordon, E. Measurement of phase gradients in the EEG. *J. Neurosci. methods* **156**, 111–128 (2006).
- Swadlow, H. A., Waxman, S. G.: Axonal conduction delays. *Scholarpedia* **1451**. (2012)
- Canolty, R. T. et al. Oscillatory phase coupling coordinates anatomically dispersed functional cell assemblies. *Proc. Natl. Acad. Sci.* **107**, 17356–17361 (2010).
- Roberts, J. A. et al. Metastable brain waves. *Nat. Commun.* **10**, 1056 (2019).
- Mahjoory, K., Schoffelen, J. M., Keitel, A., Gross, J.: The frequency gradient of human resting-state brain oscillations follows cortical hierarchies. *Elife* **9**, (2020)
- Dubey, A. & Ray, S. Cortical Electrocorticogram (ECoG) Is a Local Signal. *The. J. Neurosci. : Off. J. Soc. Neurosci.* **39**, 4299–4311 (2019).
- Raghavachari, S. et al. Theta oscillations in human cortex during a working-memory task: evidence for local generators. *J. Neurophysiol.* **95**, 1630–1638 (2006).
- Hindriks, R., van Putten, M. & Deco, G. Intra-cortical propagation of EEG alpha oscillations. *Neuroimage* **103**, 444–453 (2014).
- Neshige, S. et al. Multi-component intrinsic brain activities as a safe alternative to cortical stimulation for sensori-motor mapping in neurosurgery. *Clin. Neurophysiol. : Off. J. Int. Federation Clin. Neurophysiol.* **129**, 2038–2048 (2018).
- Tallon-Baudry, C., Bertrand, O., Delpuech, C. & Pernier, J. Oscillatory gamma-band (30-70 Hz) activity induced by a visual search task in humans. *The. J. Neurosci. : Off. J. Soc. Neurosci.* **17**, 722–734 (1997).
- Tallon-Baudry, C., Mandon, S., Freiwald, W. A. & Kreiter, A. K. Oscillatory synchrony in the monkey temporal lobe correlates with performance in a visual short-term memory task. *Cereb. cortex* **14**, 713–720 (2004).
- Zar, J. H.: *Biostatistical Analysis*. Prentice Hall (2010)

Acknowledgements

This work was supported by the Ministry of Education, Culture, Sports, Science and Technology (MEXT) KAKENHI, Grant Numbers 22H02945 and 22H03913; and the Japan Society for the Promotion of Science (JSPS) KAKENHI Grant Numbers 21K12610 and 23K18275.

Author contributions

N.S. conducted the data analysis and wrote the paper with R.M., A.S., M.O., and A.I., T.Kikuchi, T.Kunieda, and R.T. conducted all experiments. All authors contributed to the editing.

Competing interests

The Department of Epilepsy, Movement Disorders, and Physiology is an Industry-Academia collaboration course, supported by Eisai Co., Ltd, Nihon Kohden, Corporation, Otsuka Pharmaceutical Co., and UCB Japan Co., Ltd. from June 2018 to May 2023, and has been supported by Sumitomo Pharma Co., Ltd. and Nihon Kohden Corporation since June 2023. All other authors declare no competing interests.

Additional information

Supplementary information The online version contains supplementary material available at <https://doi.org/10.1038/s42003-025-09362-4>.

Correspondence and requests for materials should be addressed to Naoyuki Sato or Riki Matsumoto.

Peer review information *Communications Biology* thanks the anonymous reviewers for their contribution to the peer review of this work. Primary Handling Editor: Jasmine Pan. A peer review file is available.

Reprints and permissions information is available at <http://www.nature.com/reprints>

Publisher's note Springer Nature remains neutral with regard to jurisdictional claims in published maps and institutional affiliations.

Open Access This article is licensed under a Creative Commons Attribution-NonCommercial-NoDerivatives 4.0 International License, which permits any non-commercial use, sharing, distribution and reproduction in any medium or format, as long as you give appropriate credit to the original author(s) and the source, provide a link to the Creative Commons licence, and indicate if you modified the licensed material. You do not have permission under this licence to share adapted material derived from this article or parts of it. The images or other third party material in this article are included in the article's Creative Commons licence, unless indicated otherwise in a credit line to the material. If material is not included in the article's Creative Commons licence and your intended use is not permitted by statutory regulation or exceeds the permitted use, you will need to obtain permission directly from the copyright holder. To view a copy of this licence, visit <http://creativecommons.org/licenses/by-nc-nd/4.0/>.

© The Author(s) 2025